A novel Hopkinson-based technique for high-speed biaxial testing of sheet metals

L. Corallo[1*], P. Verleysen[1]

[1] MST-DyMaLab Research Group, Department of Electromechanical, Systems and Metal Engineering, Faculty of Engineering and Architecture, Ghent University, Technologiepark 46, 9052 Zwijnaarde, Belgium.

*Corresponding author. Email: Luca.Corallo@UGent.be

Abstract

Forming processes of sheet metals require knowledge of the material behaviour up to large levels of plastic deformation. To this purpose, biaxial bulge tests are often used. In present paper, a dynamic bulge test is presented. The testing principle relies on conventional split Hopkinson bar testing. Though, as opposed to existing setups, a different positioning of the bars leaves the sample fully accessible for optical measurements. The pressure imposed to a circular sample, together with the sample strain fields, allow to obtain reliable stress-strain data till significantly larger strains compared to tensile tests. The technique is illustrated by tests on an Al2024-T3 sheet. High speed camera imaging of the deforming sample combined with digital image processing is used to obtain full-field strain data. To quantitatively assess the added value of full-field strain measurements, stress-strain curves obtained with and without the strain data are compared.

Keywords

High-speed forming, Dynamic biaxial testing, High-speed digital imaging

1 Introduction

High speed forming of sheet metals has received more and more attention in recent decades. It does not only allow to increase the speed of production processes, though it might also be beneficial for the formability of certain metals (Verleysen et al., 2011). The design of forming processes requires knowledge of the elasto-plastic behaviour of the

involved metal up to large levels of deformation. To identify the large deformation behaviour of sheet metals, especially shear and biaxial tests are highly valuable. Both tests do not only allow to reach significantly higher deformation levels compared to conventional tensile tests, though also impose deformation states that might occur in real forming operations. Shear test results using purpose-developed sample geometries and deformation configurations presented in (Peirs et al., 2011; Traphöner et al., 2019), indeed, show that significantly higher, stable strain levels are achieved. This is also the case for biaxial tensile testing (Gutscher et al., 2004). In (Grolleau et al., 2008; Ramezani and Ripin, 2010) dynamic biaxial test techniques are presented combining a conventional split Hopkinson pressure bar (SHPB) setup with a bulge test apparatus. As is the case in SHPB setups, the sample is positioned between two long bars, i.e., the input and output bar. The circular metal sheet sample is connected to a hydraulic chamber that is in close contact with the output bar. To deform the sample, the input bar is used as a piston to pressurise the hydraulic chamber. The movement of the input bar is the result of an impact at the free end of the input bar. The pressure is measured, following Hopkinson setup principles, by strain gauges on the output bar. Major disadvantage of the existing test techniques is that the circular sample is not visible during testing. More complex material features, such as anisotropy, or test-related irregularities, such as slip or localisation of the strain in the clamping region, are not revealed. Therefore, a novel setup was developed which preserves all the advantages of Hopkinson setups and at the same time leaves the surface of the specimen fully visible during the test. Consequently, high-speed cameras can be used to capture the sample deformation. In present paper, the working principle and design of the setup are presented. Subsequently, the technique is illustrated by tests on an Al2024-T3 sheet. High speed camera imaging of the deforming sample combined with digital image processing is used to obtain full-field strain data. To quantitatively assess the added value of full-field strain measurements, stress-strain curves obtained with and without the strain data are compared.

2 The split Hopkinson bulge setup

2.1 Working principle

The main innovative feature of the split Hopkinson bulge setup presented in **Fig. 1a**, compared to existing setups (Grolleau et al., 2008; Ramezani and Ripin, 2010), originates from the special configuration of the Hopkinson bars which leaves the sample surface fully accessible for high-speed camera monitoring during the entire experiment. The 6 meter long input bar is concentrically placed inside a 3 meter long coaxial hollow tube used as output bar. The input bar is in contact with a piston, inserted into a hydraulic chamber realized inside the hollow output bar tube. Before an experiment, water is introduced into the hydraulic chamber and the input bar is placed in contact with the piston. The impact of a projectile at the free end of the input bar generates a compressive wave traveling in the input bar towards the hydraulic piston. The piston subsequently pressurizes the liquid in

the hydraulic chamber and thus deforms the sample. The sample is solidly connected to the output bar by means of a clamping system consisting of a holder, die, draw bead system, and stopper (see **Fig. 1b**). Sample and clamping system are held by ten bolts M8 to a threaded ring attached to the output bar. When the sample is deformed due to the pressure inside the hydraulic chamber, a dynamic tensile wave is transferred to the output bar. The transmitted wave traveling in the output bar is further used to derive the bulge pressure since the amplitude of the transmitted wave is proportional to the force acting on the piston.

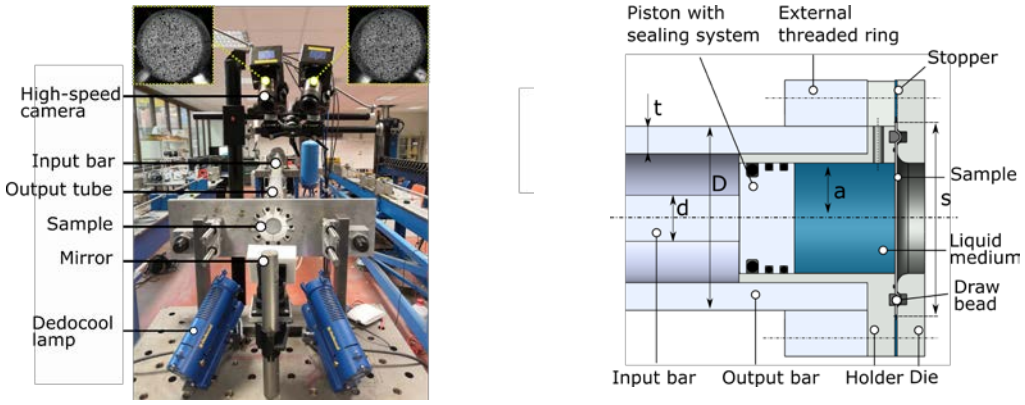

(a) (b)

Figure 1: *Split Hopkinson bar bulge setup installed at DyMaLab of Ghent University (a) and schematic representation of the components of the hydraulic chamber (b). The dimensions are the following: d=25mm, D=100mm, t=15mm, a=30mm and s=52mm.*

Both input and output bars are made of Al7075-T6 because of its high yield strength, i.e., 570 MPa, and relatively low Young's modulus, i.e., 72 GPa, which allows to impose a high-magnitude compressive wave, and thus to maximize the deformation capacity of the setup. The components of the hydraulic chamber, except for the steel stopper, are also made of high-grade aluminum to reduce the weight of the system and therefore inertia effects. The maximum duration of an experiment is approximately 1.2ms. The parameters referring to the input and output bars are further indicated with the subscripts *inp* and *out*, respectively. Global experimental data, such as the pressure acting at the sample surface and the piston displacement, are derived from the strain gage measurements on the Hopkinson bars. Indeed, the strain histories ε_i, ε_r and ε_t, corresponding with the incident, reflected and transmitted waves, respectively, are recorded by strain gages attached to the bars. Assuming the same material for both input and output bar, the piston displacement Δd imposed to the sample can be calculated from the displacements of the bar interfaces:

$$\Delta d(t) = U_{inp}(t) - U_{out}(t) = C\int_0^t \varepsilon_i(\tau) - \varepsilon_r(\tau) - \varepsilon_t(\tau)\, d\tau \qquad (1)$$

Where U indicates the bar/sample interface displacement and C the one-dimensional wave propagation speed in the slender Hopkinson bars. The bulge pressure is derived

considering the equilibrium between the bulge pressure and the tensile force F_{out} acting on the output bar during the sample deformation:

$$p(t) = \frac{F_{out}(t)}{A_p} = \frac{A_{out}\,\sigma_t(t)}{A_p} = \frac{A_{out}\,E_{out}\,\varepsilon_t(t)}{A_p} \tag{2}$$

E is the Young's modulus. A_{out} and A_p are the sections of the output bar and piston, respectively. The material sample is a thin circular plate with initial thickness t_0 clamped around its edge to a circular die of diameter 2a (see **Fig. 1b**). It is often assumed that the specimen deforms into a quasi-spherical cap with a polar height h by a hydrostatic pressure p acting at one side of the specimen surface (see **Fig. 2**).

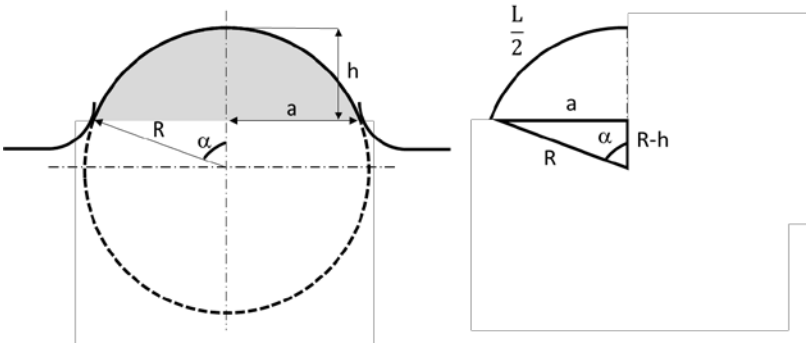

***Figure 2**: Schematic representation of an assumed spherical sample deformation during a bulge experiment.*

Assuming an isotropic material, and thus axisymmetric deformation, the membrane stress at the sample apex is described by equation (Hill, 1950):

$$\sigma = \frac{pR}{2t} \tag{3}$$

Where R is the radius of the deformed sample. Even if the sample does not deform as a sphere, **Eq. 3** can still be used with the local radius of curvature at the apex. t is the actual thickness which can be calculated from the true thickness strain. This strain is equal to the equivalent strain quantified by DIC or can be approximated using the spherical cap deformation assumption as further elaborated in section 2.2.

2.2 Sample deflection and strain calculation from Hopkinson measurements

The strain and thickness calculated locally at the apex by DIC can alternatively be obtained assuming that the sample deforms into a spherical cap at every stage of the deformation. Piston, hydraulic chamber and die all have the same circular section with radius a (see Fig. 1b). If the sample deforms as a spherical cap, the volume of liquid displaced $A_p\Delta d$ is equal to the volume of the cap:

$$A_p \Delta d(t) = \frac{\pi h}{6}(3a^2 + h(t)^2) \quad (4)$$

Solving the above equation for h gives an approximation for the deflection at the sample apex given by:

$$h(t) = \sqrt[3]{3a^2\Delta d(t) + \sqrt[2]{(3a^2\Delta d(t))^2 + a^6}} + \sqrt[3]{3a^2\Delta d(t) - \sqrt[2]{(3a^2\Delta d(t))^2 + a^6}} \quad (5)$$

In a real test, the spherical cap deformation is only reached, with a reasonable approximation, after a certain deformation in the plastic domain. For the test configuration considered in present study, finite element calculations have shown that an apex displacement of 3.2mm is needed. The corresponding piston displacement is found to be equal to 3.7mm. Therefore, to increase the accuracy of **Eq. 5**, it is only used after reaching the threshold deformation and the piston displacement considered is the increment from that moment $\overline{\Delta d}(t)$. Once, the h(t) is calculated, W=3.2mm is added to obtain an apex out-of-plane displacement that can be compared to the corresponding value obtained by DIC:

$$\bar{h}(t) = \sqrt[3]{3a^2\overline{\Delta d}(t) + \sqrt[2]{\left(3a^2\overline{\Delta d}(t)\right)^2 + a^6}} + \sqrt[3]{3a^2\overline{\Delta d}(t) - \sqrt[2]{\left(3a^2\overline{\Delta d}(t)\right)^2 + a^6}} + W \quad (6)$$

Eq. 6 is not valid in the early stages of deformation. **Eqs. 7, 8** can be used to determine the (assumed constant) radius of curvature R and the angle α, respectively (see **Fig. 2**):

$$R = \frac{a^2 + h^2}{2h} \quad (7)$$

$$\alpha = \cos^{-1}\left(1 - \frac{h}{R}\right) \quad (8)$$

The equivalent strain can be calculated as:

$$\varepsilon = 2ln\left(\frac{L}{2a}\right) \quad (9)$$

Where L=(2α)R is the actual length of the sample profile at a specific stage of deformation. The corresponding actual thickness t is found as:

$$t = t_0\left(\frac{2a}{L}\right)^2 \quad (10)$$

3 Experimental procedure

High-speed bulge experiments are performed on 0.8mm thick Al2024-T3 sheet. Al2024 is widely employed in the forming industry because of its good machinability, relatively high

ultimate tensile strength, and low density. Before an experiment, a stochastic white/black speckle pattern is applied to the sample surface. The sample surface is continuously recorded during an experiment using two high-speed cameras. The cameras used are Photron mini AX200 cameras equipped with two Tamron lenses of 90mm focal length. The cameras are used together with a mirror with high surface quality placed in front of the sample while its surface is illuminated by two Dedocool lamps (see **Fig. 1a**). From the recorded images, full-field displacement and strain fields are extracted using the 3D commercial DIC software provided by MatchID. A framerate of 30 000 fps is chosen giving images with a spatial resolution of 512 x 384 pixels. The order of magnitude of the resolution is of about 10^{-3} mm and 10^{-4} for the displacement and strain fields respectively. The procedure used to determine the flow curve of the tested material is based on the ISO16808:2014 standard.

4 Results and discussion

In the following sections, detailed results are presented for a high-speed bulge test performed using an impactor velocity of 16.5 m/s. All results obtained by stereo DIC measurements are referred to as DIC, the results derived using geometrical approximations, i.e., equations derived in section 2.2, as Hopkinson.

4.1 Sample out-of-plane displacement

In **Fig. 3** the sample profiles measured via DIC along two central lines aligned with the rolling and transverse direction are presented at several time instants, together with best fitted circles with radius R. The assumption that the specimen deforms as a spherical cap, employed to derive the equations in section 2.2, is only valid at the initial stage of the experiment. Indeed, at higher deformation levels, the radius around the apex is smaller than in the surrounding material. No significant differences are observed between the profiles, radii included, along the rolling and transverse direction. The DIC and analytical out-of-plane displacements at the sample apex are reported in **Fig. 4**. DIC measurements are corrected to account for the rigid motion of the output tube. The initial upwards shift of the displacement obtained via Hopkinson measurements is related to the use of the constant corrective parameter W. The out-of-plane displacement calculated via Hopkinson measurements is in good agreement with that one quantified by DIC. The evolution of the bulge pressure (**Eq. 2**) with respect to the out-of-plane displacement at the sample apex from DIC and Hopkinson measurements is shown in **Fig. 5**. The good agreement between the results derived by DIC and Hopkinson measurements supports the employment of the analytical approach to quantify both the sample deflection at the sample apex and the evolution of the bulge pressure with respect the out-of-plane displacement.

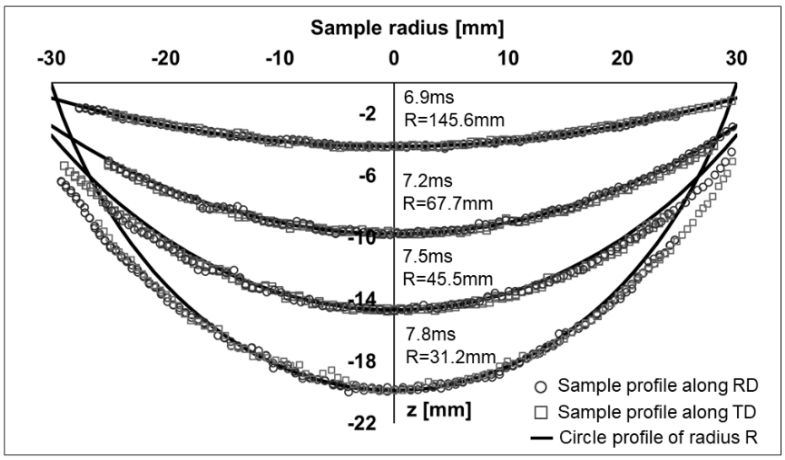

Figure 3: *Sample profile along the central lines aligned with the rolling and transverse direction and best fitted circles with radius R at different instants of the test.*

Noticeable fluctuations are observed in both **Fig. 4** and **Fig. 5**, for the data obtained by DIC. Detailed analysis of the high-speed camera images has revealed sample vibrations during the high-speed bulge test. The influence of sample ringing on the stress-strain curve is further discussed in section 4.3.

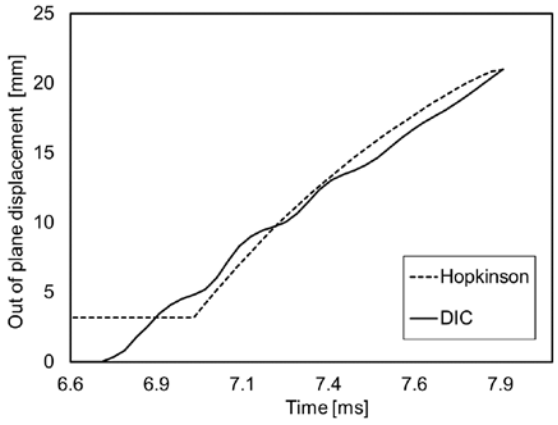

Figure 4*: Out-of-plane displacements at the sample apex.*

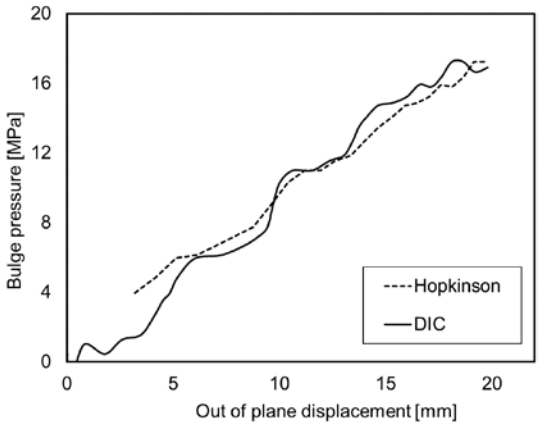

Figure 5: *Evolution of the bulge pressure with respect to the sample displacement at the sample.*

4.2 Strain and strain rate

DIC contour plots of the rolling and transverse strains are compiled in **Fig. 6.** Differences between the two strain components are observed in terms of strain amplitudes and distribution. The highest strain values are found at the sample apex. The fracture starts at the apex and propagates along the rolling direction. The images confirm that no undesirable concentration of deformation occurs at the sample clamping. The strain fields, during the last stages of the experiment (7.8-7.9ms), exhibit an elliptical distribution. Indeed, the strain in the rolling direction has a higher intensity along the transverse direction. On the contrary, the strain in the transverse direction is higher along the rolling

direction. The differences between the two strain fields give a clear indication of the material anisotropy.

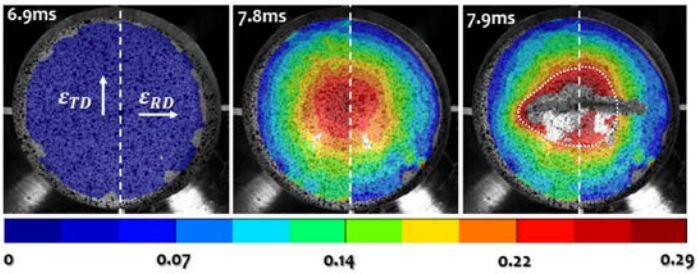

***Figure 6**: Full-field contour plots of strain in the rolling (right side images) and transverse (left side images) directions, i.e., RD and TD, respectively, at three instants during the test.*

The strain histories quantified by DIC and Hopkinson measurements are reported in **Fig. 7**. While DIC allows to quantify the strain history from the beginning of the experiment, the analytical approach can be used only once the sheet metal starts deforming as a spherical cap. Indeed, the time delay of the dashed curve in **Fig. 7** is relative to the initial deformation needed to bring the sample in contact to the die. Furthermore, the onset of strain concentration at the sample apex, and the following increment of strain during the final stage of the experiment, can only be detected employing optical measurement technique. The strain rate histories reported in **Fig. 8** are calculated as time derivative of the strain.

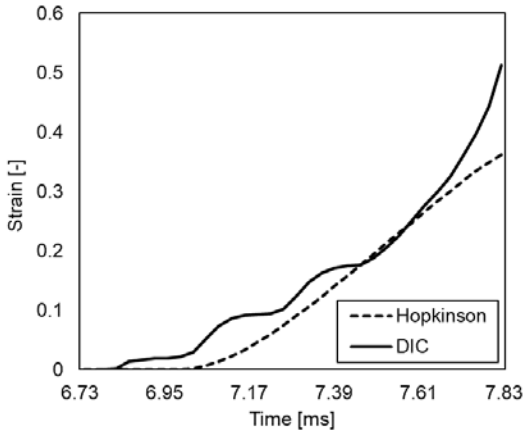

***Figure 7**: Strain evolution with respect to the time.*

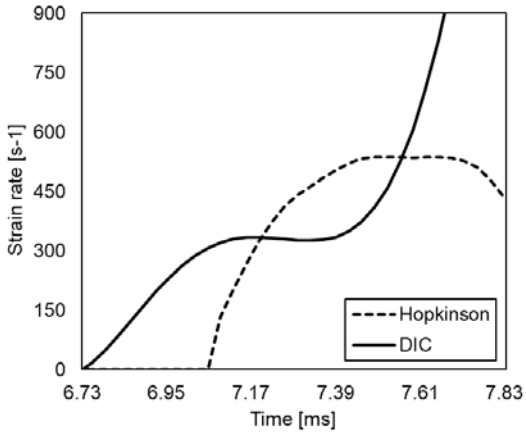

***Figure 8**: Strain rate evolution with respect to the time.*

After a stable plateau ranging between 300-350s^{-1} the strain rate measured by DIC increases very rapidly until fracture of the sample. The significant increment in strain rate is linked to the concentration of strain around the sample apex, as observed in **Fig. 6**. Hopkinson results instead, show a quasi-constant strain rate of about 550s^{-1}, after which the strain rate decreases. The same observations made for the strain history concerning the time delay and the capability of detecting the strain localization are also valid for the strain rate**.** The comparison between Hopkinson and DIC results show as the analytical approach cannot be used to extract information concerning the evolution of strain and strain rate.

4.3 Material flow curve

The material flow curves are calculated using the equation introduced in section 2. Strain gage recordings on the output bar allow to measure the bulge pressure during the experiment, while the actual thickness and the radius of curvature can be derived using direct DIC measurements or via analytical approximations. **Eq. 3** can be successfully employed to derive the biaxial stress in dynamic loading conditions since it relies on online measurements of the sample deformation, i.e. R and t, and bulge pressure. The nature of the dynamic experiment does not influence the validity of the equation. In **Fig. 9**, the stress-strain curves are derived using both the approaches. The high value of stress observed at the beginning of the curve obtained without DIC is related to the initial extremely high value of the radius of curvature. While the stress amplitude is comparable for the two curves, the value of deformation at fracture measured using DIC is remarkably higher. Indeed, the analytical approach does not account for the onset of a strain gradient along the sample radius**.** Noticeable oscillations are observed in the stress level, especially during the initial stage of the experiment. Since the bulge pressure increases gradually without noticeable oscillations, the oscillations originate from variations in R and t measured by DIC. Further analysis has revealed that during the initial stage of the experiment the sample starts vibrating. The ringing of the sample has a direct impact on the radius of curvature, especially during the first stage of the experiment.

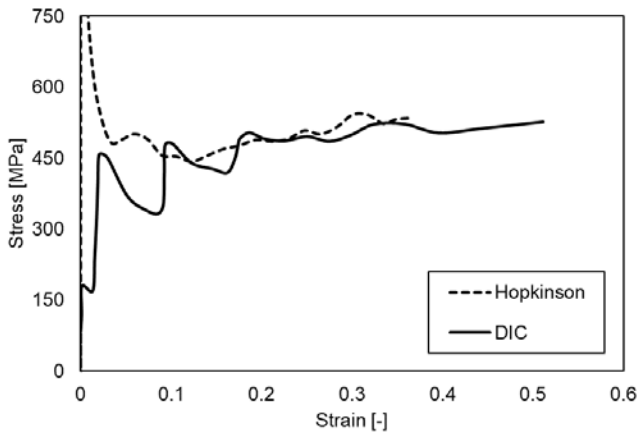

Figure 9*: Stress-strain curve obtained from high-speed bulge test.*

5 Conclusions

In this work a novel split Hopkinson bar bulge test facility is presented. The special configuration of the Hopkinson bars leaves the sample surface fully accessible for high-speed camera monitoring during the entire experiment. An analytical formulation to quantify the sample deformation, including the apex out-of-plane displacement and strain are proposed and compared with the results obtained by DIC processing. Strain gage measurements on the bars can be successfully used to quantify the apex out-of-plane displacement and its evolution with respect to the bulge pressure. However, the analytical

approach reveals a low accuracy in the prediction of the strain and strain rate histories. Furthermore, the employment of full-field stereo DIC reveals additional features on the material behaviour and sample response, such as material anisotropy and sample vibration. To quantitatively assess the added value of full-field strain measurements, stress-strain curves obtained with and without the strain data are compared. Hopkinson measurements cannot be employed to describe the flow curve up to large level of deformation since the analytical approach does not account for the strain localization at the sample apex. The synergy between traditional, Hopkinson-based strain gage and stereo DIC measurements, shows the potential of the setup to be employed as a valid dynamic counterpart of the quasi-static bulge experiment.

6 Acknowledgments

The authors gratefully acknowledge the Research Foundation Flanders-FWO, application number 1SC5619N. The authors thank the Ghent University technical staff Wouter Ost, Luc Van den Broecke and Pascal Baele for their valuable support for the realization of the setup.

References

Grolleau, V., Gary, G., Mohr, D., 2008. Biaxial testing of sheet materials at high strain rates using viscoelastic bars. Exp. Mech. 48, 293–306.

Gutscher, G., Wu, H.-C., Ngaile, G., Altan, T., 2004. Determination of flow stress for sheet metal forming using the viscous pressure bulge (VPB) test. J. Mater. Process. Technol. 146, 1–7.

Hill, R., 1950. C. A theory of the plastic bulging of a metal diaphragm by lateral pressure. Lond. Edinb. Dublin Philos. Mag. J. Sci. 41, 1133–1142.

Peirs, J., Verleysen, P., Van Paepegem, W., Degrieck, J., 2011. Determining the stress–strain behaviour at large strains from high strain rate tensile and shear experiments. Int. J. Impact Eng. 38, 406–415.

Ramezani, M., Ripin, Z.M., 2010. Combined experimental and numerical analysis of bulge test at high strain rates using split Hopkinson pressure bar apparatus. J. Mater. Process. Technol. 210, 1061–1069.

Traphöner, H., Clausmeyer, T., Tekkaya, A.E., 2019. Methods for measuring large shear strains in in-plane torsion tests. J. Mater. Process. Technol. 116516.

Verleysen, P., Peirs, J., Van Slycken, J., Faes, K., Duchene, L., 2011. Effect of strain rate on the forming behaviour of sheet metals. J. Mater. Process. Technol. 211, 1457–1464.